Check for updates

JGR Solid Earth

RESEARCH ARTICLE
10.1029/2020JB021341

The Effects of 180 years of Aging on the Physical and Seismic Properties of Partially Saturated Sands

Vanshan Wright[1,2] **and Matthew Hornbach**[1]

[1]Roy Huffington Department of Earth Sciences, Southern Methodist University, Dallas, TX, USA, [2]Department of Geology and Geophysics, Woods Hole Oceanographic Institution, Woods Hole, MA, USA

Key Points:

- Elastic moduli of recently deposited sands at Port Royal Beach increase with age for at least 180 years
- Time-dependent increases to the elastic moduli of Port Royal sands are not solely explained by mechanical compaction
- Elastic moduli of these sands most likely increase with age due to grain reorganization that leads to higher grain contact friction

Supporting Information:

Supporting Information may be found in the online version of this article.

Correspondence to:

V. Wright,
vwright@whoi.edu

Citation:

Wright, V., & Hornbach, M. (2021). The effects of 180 years of aging on the physical and seismic properties of partially saturated sands. *Journal of Geophysical Research: Solid Earth*, *126*, e2020JB021341. https://doi.org/10.1029/2020JB021341

Received 12 NOV 2020
Accepted 6 MAY 2021

Abstract Constraining how the physical properties and seismic responses of recently deposited sands change with time is important for understanding earthquake site response, subsurface fluid flow, and early stages of lithification. Currently, however, there is no detailed (cm-scale) assessment of how sand's physical properties and associated seismic velocities evolve over the first two centuries after deposition. Here, we integrate sedimentation rates with seismic velocity and sediment physical properties data to assess how the vadose zone sands at Port Royal Beach, Jamaica, change within 180 years after deposition. We show that compressional and shear wave velocities increase with sediment age, whereas porosity, grain size, sorting, mineralogy, and cementation fraction remain relatively unchanged during the same period. Rock physics models (constrained by the measured physical properties) predict constant seismic velocities at all sites regardless of sediment age, though misfits between modeled and observed velocities increase with sediment age. We explain these misfits by proposing that shallow sands undergo microstructural grain reorganization that leads to a more uniform distribution of grain contact forces with time. Our results imply that beach sands undergo a previously undocumented lithification process that occurs before compaction.

Plain Language Summary Sands change after being deposited. Their porosity (i.e., volume of pore space) reduces, the average number of grains contacting each other increases, and chemical reactions may cause the grains to adhere more firmly. These changes influence how strong sands are, how resistant they are to being deformed by earthquakes, the ability for fluids to flow through sands, and how quickly sands transition to rocks. For many years, scientists believed that porosity reduction was the dominant non-chemical way sands change and become stronger. Forty years ago, researchers observed something quite enigmatic – the strength of artificial sands increase within minutes after being deposited. This strengthening lasted for three decades and occurred without significant porosity reductions. Until now, it was unclear what controls this process, whether it lasts longer than decades, and whether it occurs in natural beach sands. This paper argues that, within the first 180 years after deposition, natural sands at Port Royal Beach in Jamaica strengthen due to grain rotation, slippage, and rolling that increase contact area and stress between the grains without reducing porosity significantly. The new paradigm developing is that recently deposited shallow sands more significantly change via this grain reorganization process versus porosity reduction.

1. Introduction

The physical properties and seismic velocities of shallow sediments vary with depth and time since deposition (Atkins & McBride, 1992; Prodger et al., 2016; Pryor, 1973). Variations exist in sediment porosity, bulk density, sphericity, sorting, grain size, rounding, fluid saturation, cement fraction, and seismic velocities (Atkins & McBride, 1992; Gunn et al., 2006; McLean & Kirk, 1969; Prodger et al., 2016; Pryor, 1973; Vousdoukas et al., 2007). Variations in sediment properties control subsurface fluid flow and sediment strength and are crucial for understanding slope stability, earthquake-induced liquefaction, seawater intrusion and upwelling, sediment lithification, and the development of oil and gas reservoirs (Crowe & Milne, 2013; Dugan & Flemings, 2002; Lundegard, 1992; Morelock, 1969).

With increased burial, sediments typically experience effective stress-induced porosity reductions that cause increases in bulk density, the average number of grain-grain contacts per particle (coordination number), elastic moduli, and seismic velocities (Athy, 1930; Dutta et al., 2009; Murphy, 1982; Revil et al., 2002). This

© 2021. American Geophysical Union. All Rights Reserved.

process (mechanical compaction) is well-documented with direct measurements in deep (>100 m) marine sediments (e.g., Athy, 1930; Dutta et al., 2009). However, porosities of well-sorted, medium-grained beach, river, and dune sediments remain constant with depth down to at least 17 m (0.47–0.49 for 174 samples) (Atkins & McBride, 1992; Pryor, 1973). Coordination numbers of these sands slightly increase with depth (from ~1 to 2 for 50 samples down to 17 m) despite porosities remaining constant (Atkins & McBride, 1992). These observations contradict expectations that porosity reduction is the primary cause of increases in coordination number with depth (Athy, 1930; Dutta et al., 2009; Murphy, 1982; Revil et al., 2002).

Time since deposition influences the physical properties of shallow sediments. Seasonal variations in beach grain size and sorting correlate with changes in sediment source, wind strength, currents, and wave conditions (Prodger et al., 2016). Freshly deposited artificial sands, silt-laden tailing, and sand columns recreated in the lab experience increases to their shear moduli that begin within minutes after deposition, last for days to 1–4 decades, and are not solely attributed to porosity reduction—porosity typically changes by less than 3% during the same period (Dumas & Beaton, 1988; Mesri et al., 1990; Mitchell & Solomayor, 1984; Troncoso & Graces, 2000). Since the first observation of this processes ~40 years ago, studies have hypothesized but have yet to show definitively in the field that time-dependent increases to sediment shear moduli could be the result of increased cementation or grain reorganization that leads to increased friction at grain contacts (Bowman & Soga, 2003; Mitchell, 2008). Presently, it is unclear whether natural clean (<5% fines) sands also experience similar age-dependent shear moduli changes, what controls the process, and whether it lasts longer than decades (Mitchell, 2008).

A feasible way to study centennial-scale sediment changes involves making measurements along a coastline-to-inland transect at a prograding beach whose sediment source has not changed for centuries (Figures 1–5). Spatiotemporal sediment changes would be evidenced by statistically significant increases or decreases to seismic velocities and or core-measured properties (e.g., porosity, bulk density, grain size, cement fraction, saturation, and mineralogy). It is also reasonable to infer that the grain or fluid microstructures are different between study sites if the core-measured physical properties cannot explain changes in seismic velocities.

Comparisons between measured and predicted seismic velocities from Hertz-Mindlin's rock physics model (Mindlin, 1949) could provide first-order insights into how changes in the sediments' microstructures influence seismic velocities. This rock physics model approximates sands as randomly organized groups of identical spheres whose grain contact forces are uniformly distributed and quantifiable using Hertzian-contact mechanics (Mindlin, 1949). Unlike the other six granular media rock physics models where there has been little to no ground-truthing work to understand causes for seismic velocity mispredictions, studies show that mispredictions from Hertz-Mindlin's rock physics models are attributable primarily to nonuniform distributions of contact forces introduced by variations in coordination number, contact geometries, and force chain links in natural sands (Makse et al., 1999, 2004; Bachrach & Avseth, 2008). By combining Hertz-Mindlin's rock physics model insights into sediment microstructure with coring and seismic velocity data, one achieves a relatively comprehensive way of quantifying spatiotemporal sediment changes.

We perform a cm-scale assessment of how vadose zone sands (upper 2.2 m) at Port Royal Beach, Jamaica, change within 180 years after deposition. This prograding beach is scientifically appropriate for our study because the beach's sediment deposition, erosion, and liquefaction histories are well-documented, and there exist legacy maps for constraining sediment age at decadal resolutions (Fuller, 1907; Goreau & Burke, 1966; McDonald et al., 2013). We interpret that its sands experience grain reorganization (i.e., rolling, slipping, and rotation) that leads to changes in grain positions and contact geometries, which then lead to more uniform distributions of contact forces but no significant changes to porosity. This grain-reorganization process is more dominant than porosity-reducing mechanical compaction at controlling the strength, seismic velocity, and porosity of sands during their first 180 years after deposition.

2. Methods

We use t-tests and Monte-Carlo analyses to identify spatiotemporal changes between sediment age, seismic velocities, and physical properties at four sites (sites1-4) at Port Royal Beach (Figure 1). We constrain sediment ages using legacy maps and topographic surveys. We constrain mineralogy, grain size, sorting,

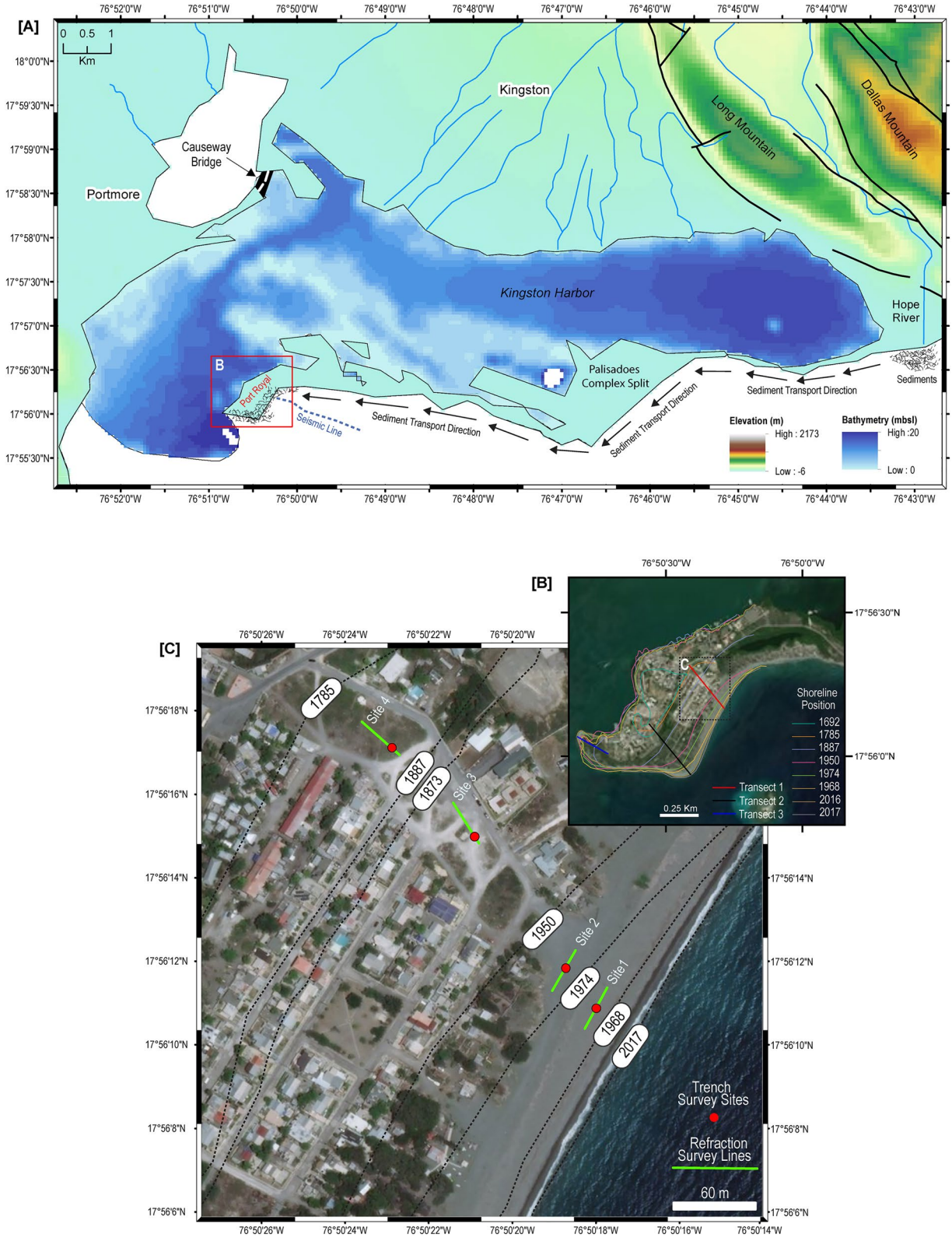

Figure 1. (a) Map of Port Royal Beach. (b) Map showing shoreline positions and transects where we estimate progradation rates (Figure S1).

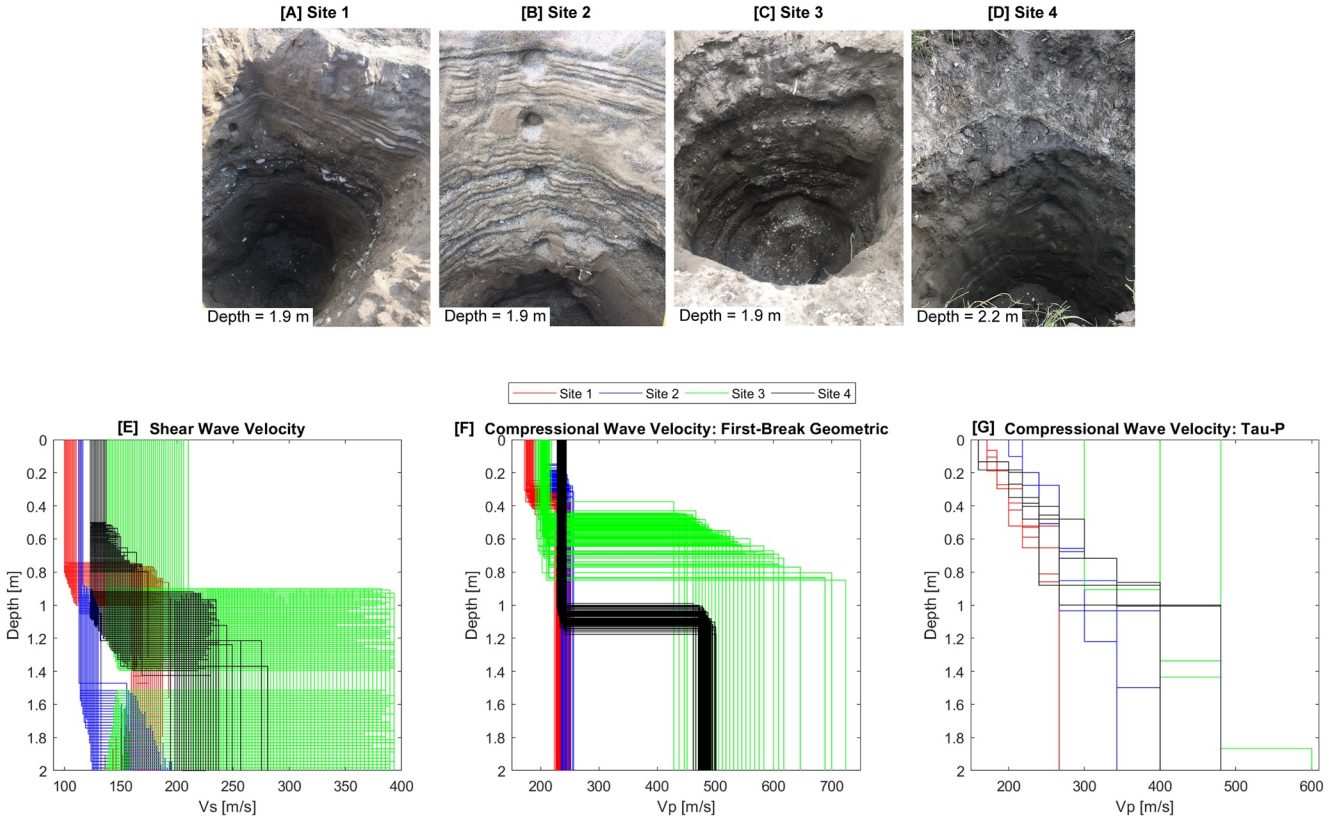

Figure 2. (a–d) Photos show trench sites 1–4. (e) Surface wave tomography-based (Figure S2) V_s (f) V_p estimated with Wiechert-Herglotz solution (Tau-p). (g) V_p based on the first-break geometric method.

sphericity, roundness, porosity, bulk density, and cement fraction from trench sidewall cores. We measure and model seismic velocities using refraction surveys and Hertz-Mindlin's rock physics model (Mindlin, 1949), respectively.

2.1. Constraining Sediment Age

We constrain sediment age using three-dimensional time contours derived from the beach's paleo shoreline, submarine and subaerial slope surveys, and sea-level curves (Figures 1 and S1). We digitize paleo shorelines from georeferenced maps of Port Royal dated to 1692, 1782, 1785, 1873, 1876, 1887, 1950, 1968, and 1974 using 425-year-old (or older) buildings, roads, and landmarks as control points (e.g., Port Royal Navy Hospital, Fort Charles, St. Peters Anglican Church, and High Street). Affine transformations during the georeferencing produce shoreline position uncertainties of 3–13 m. We account for these uncertainties by calculating sediment age for all possible combinations of shoreline positions. Where possible, we also randomly remove 1–2 control points and assess their influences on the shoreline positions. While creating the time contours, we also assume that the submarine and subaerial beach slopes remained constant over the last two centuries because (a) this is what historical elevation and bathymetric maps show, (b) deposition rates were primarily controlled by long-shore drift and easterly winds during this period (Goreau & Burke, 1966; Wright et al., 2019), and (c) Jamaica's local sea level has remained constant for at least 425 years (Digerfeldt & Hendry, 1987). We interpolate between the contours to estimate sediment ages at sites 1–4.

2.2. Sediment Collection and Physical Property Analyses

We dug 1.8–2.2 m deep trenches at sites 1–4 and used aluminum cans (mostly 10 cm high by 6 cm wide) to collect 1–3 sidewall samples from the middle of each bed (Figures 2a–2d). We collected a total of 10, 11, 9, and 9 samples from sites 1–4, respectively. After collection, we immediately covered and stored the samples,

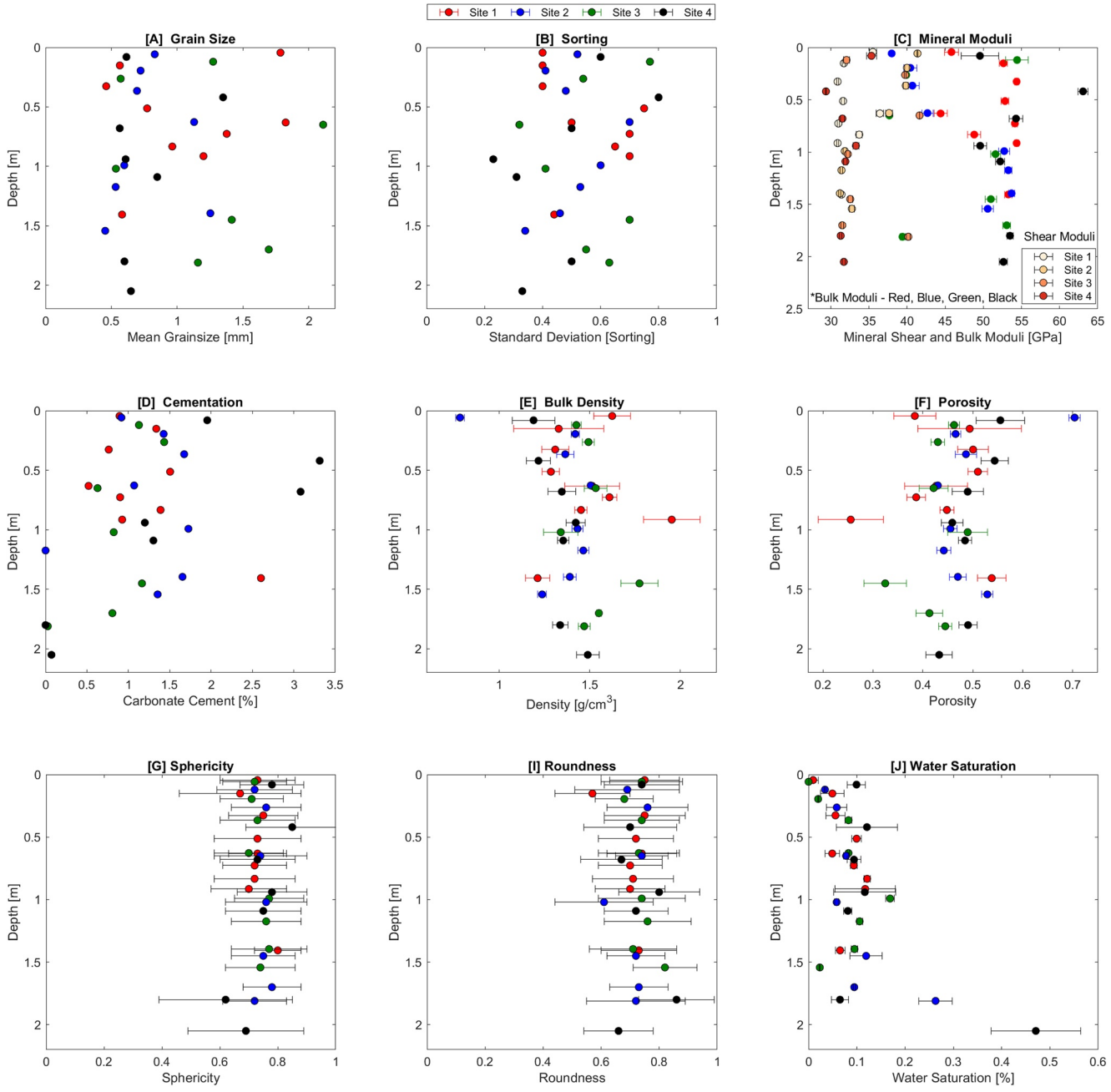

Figure 3. (a–i) Core physical properties results with 1-sigma uncertainties—also see Figure S3 and Table S1.

weighing them within ~1–30 minutes. We dried the samples in an oven for at least 8 h before re-weighing them to estimate wet and dry weights.

We assessed mineralogical changes using x-ray diffraction (XRD), scanning electron microprobe, optical microscopy, and pictomicrographic analyses. During XRD analyses, we used the PDF-4+ International Center for Diffraction Data library as a reference for identifying minerals and calculated relative percentages using the reference intensity ratio method (Hillier, 2000). We quality control XRD results by inspecting the unaltered sediments with an optical microscope, pictomicrograph, and a scanning electron microprobe, which help distinguish between detrital calcium carbonate versus cement; calcite cement was <1% of the calcium carbonates (Figures 3 and S5). We quantified carbonate percentage by measuring sand mass changes after saturating 40–100 g of each sample in 10% diluted hydrochloric acid for at least 24 h.

We estimated grain size and sorting using the Folk and Ward (1957) and a stochastic numerical grain recreation method. First, we used a mechanical shaker and sieving to bin the sediments based on grain size. Approximately 61% of the samples have bimodal or trimodal grain size distributions, with the remaining 39% being unimodal. Since the Folk and Ward (1957) method yields erroneous sorting estimates for non-unimodal samples, we also estimated grain size and sorting numerically. We began by approximating the samples as a group of perfect spheres whose total mass equals the weighed mass of the retained sediments in each sieve and whose diameters are within each sieve's range. We performed this analysis 10,000 times, representing the mean grain size as the radius of the mean weighted mass for the entire reconstructed sample and sorting as the weighted standard deviation. The perfect sphere assumption is valid as 30–50 grains from each bed have mean sphericities of 0.7–0.8 on a scale of 0–1, where one refers to a perfect sphere (Figure 3g). Folk and Ward (1957) and our numerical approach produce an average difference in grain size of ∼0.2 mm or ∼26.2%. We quantified grain sphericity and roundness using the methods of Zheng & Hyrciw (2015). Sphericity and roundness uncertainties derive from their standard deviations.

We used the samples' mass, volume, and mineralogy to estimate bulk density, porosity, and water saturation. Bulk density is the mass of the wet sand divided by its volume. Porosity is one minus the ratio of the samples' dry-frame bulk density and mineral density, and water saturation is the quotient of pore water volume and pore volume. We calculated average mineral densities using the arithmetic mean, assuming that the densities of quartz, albite, and calcite (i.e., the three minerals within the sediments) are 2.65, 2.62, and 2.71 g/cm^3, respectively (Katahara, 1996; Prasad et al., 2002; Wang et al., 1998). The bulk density, porosity, and water saturation uncertainties derive from the variances in measured mass, volume, and mineralogy.

2.3. Seismic-Refraction Data Collection and Velocity Analysis

We constrained V_p by analyzing the waveforms collected during 24-channel reverse refraction surveys. The geophones have corner frequencies of 4.5 Hz, the receiver spacing was 0.3 m, and the source offset was 0.3–19 m (incrementing by 3 m). The source was a 16 lb. hammer that strikes an aluminum plate 10 times to increase the signal-to-noise ratios. To create V_p travel-time curves, eight seismologists at Southern Methodist University picked first-arrivals, and the first author picked first-arrivals at 3–5 separate times within three months. We (the authors) estimate V_p (from travel-time curves) using the first-break geometrical method and Wiechert-Herglotz solution for horizontal components of turning wave velocities (Batemann, 1910; Herglotz, 1907; Wiechert, 1910; Wiechert & Geiger, 1901). We determine velocity uncertainties by randomizing the first-arrival picks used in the travel-time curves.

We estimated V_s using multichannel analyses of the surface waves collected during 24-channel refraction surveys with receiver spacings and shot offsets of 1.5 and 7 m, respectively. We calculated dispersion curves using the phase shift method (Park et al., 1999) and inverted for V_s structure using Geopsy's (www.geopsy.org) neighborhood algorithm (Wathelet et al., 2004). We perform three sets of inversion per dispersion curve—these inversions run for 25,000, 35,000, or 50,000 times. Each new inversion begins with 5,000 randomly generated models that are constrained by the dispersion curve and empirical relationships between V_s and surface wave dispersion. Specifically, we set V_s to respectively 1 and 1.16 times the minimum and maximum phase velocity of the surface waves (consistent with Richart et al., 1970), V_p to 150–2,500 m/s, Poisson's ratio to 0.2–0.5, and bulk density to 1,500 g/cm^3. We use Cox and Teague (2016)'s layer ratio method to create five separate layer thickness input models. We set the depth of the shallowest and deepest layer to 0.2–0.3 times the minimum and maximum wavelengths of the surface waves, respectively. The thickness of the layers beneath the shallowest one consistently increases by a ratio of either 1.2, 1.4, 1.6, 1.8, or 2.0 times the thickness of the shallowest layer. We did not use measured bed thickness to constrain the solutions because doing so would over parameterize an already non-unique and ill-posed inversion problem; beds are not resolvable with the seismic data because the beds are smaller than 0.2 times the minimum wavelength of the surface waves. After using the Haskell-Thomson method (Haskell, 1951; Thomson, 1950) to calculate dispersion curves for the proposed model solutions, we calculate the misfits between modeled and observed dispersion curves using the root mean squared error before performing 5000 random walks, which function to avoid local minima when a new set of 5000 models are generated. Our solutions are the 1000 best-fit models taken from the layer thickness model with the lowest corrected Akaike information criteria score.

2.4. Seismic Velocity Predictions From Rock Physics Modeling

We calculate compressional and shear wave velocities using Equations 1 and 2, where ρ_b, K_{eff}, and μ_{eff} represent bulk density, effective bulk modulus, and effective shear modulus, respectively. We estimate K_{eff} and μ_{eff} from Hertz-Mindlin's rock physics model (Mindlin, 1949, Equations 3–9) and Biot-Gassmann theory (Biot, 1956; Gassmann 1951; Equation 10). ρ_b is from the sediment core analyses.

$$Vp = \sqrt{\frac{K_{\text{eff}} + (4/3)\mu_{\text{eff}}}{\rho_b}}, \tag{1}$$

$$Vs = \sqrt{\frac{\mu_{\text{eff}}}{\rho_b}}. \tag{2}$$

Hertz-Mindlin provides estimates on dry-frame bulk and shear moduli. The model requires (a) porosity $Ø_z$, (b) effective pressure P_{eff} estimated from Equation 5 where g, ρ_b, z, W_d, Y_w, and S_w respectively refer to acceleration due to gravity, bulk density, sample depth, water depth, unit weight of water, and fluid saturation percentage, (c) mineral bulk k_m and shear μ_m moduli derived from Voigt M_v and Reuss M_R bounds (i.e., Equations 6 and 7 where f_i and m_i respectively refer to fractional proportions and elastic moduli of the ith mineral) (Hill, 1952), (d) mineral poisons ratio η_m derived from Equations 8 and (e) average coordinate numbers c derived from Equation 9 (Murphy, 1982), and the volume fraction of rough to smooth grain contacts ft, where rough (smooth) grain contacts are ones that resist entirely (allows) tangential slip during seismic wave propagation.

$$K_{\text{HM}} = \left[\frac{c^2(1-Ø_z)^2 k_m{}^2}{18\pi^2(1-\eta_m)^2} P_{\text{eff}}\right]^{1/3}, \tag{3}$$

$$\mu_{\text{HM}} = \frac{2+3ft-\eta_m(1+3ft)}{5(2-\eta_m)}\left[\frac{3c^2(1-Ø_z)^2(4)\mu_m^2}{2\pi^2(1-\eta_m)^2}\mathrm{P}_{\text{eff}}\right]^{1/3}, \tag{4}$$

$$P_{\text{eff}} = g\int_0^z \rho_b(z)\,dz - \left[z - W_d\right]S_w Y_w, \tag{5}$$

$$M_v = \sum_{i=1}^{N} f_i m_i, \tag{6}$$

$$\frac{1}{M_R} = \sum_{i=1}^{N} \frac{f_i}{m_i}, \tag{7}$$

$$\eta_m = \frac{3k_m - 2\mu_{\text{m}}}{6k_m + 2\mu_{\text{m}}}, \tag{8}$$

$$c = 20 - 34Ø_z + 14Ø_z^2. \tag{9}$$

We used the Gassmann-Biot theory (Biot, 1956; Gassmann, 1951; Equation 10) to calculate the effects of fluid saturation on dry-frame bulk moduli. This method assumes that sediments are heterogeneous and

fluids are not flowing (Biot, 1956; Gassmann, 1951). In the equation, K_{air} represents the bulk modulus of air (0 kPa) and K_{f2} represents the bulk modulus of sediments filled with a mix of seawater (2.3 GPa) and air. We determine bulk moduli using Equations 6 and 7.

$$\frac{K_{\text{eff}}}{K_m - K_{\text{eff}}} - \frac{K_{f2}}{\text{Ø}_z\left(K_m - K_{f2}\right)} = \frac{K_{\text{HM},W}}{K_m - K_{\text{HM},W}} + \frac{K_{\text{air}}}{\text{Ø}_z\left(K_m - K_{\text{air}}\right)} \tag{10}$$

From Equations 1–10, we calculated seismic velocities 10,000 times using parameters and assumptions that minimize uncertainties that arise from using core-point measurements to predict bulk-averaged measured seismic velocities within each trench. For each calculation, we randomly select new parameter values that are between the maximum and minimum estimates of all point measurements of the input parameter per bed (e.g., Ø_z and ρ_b). We assume that the point measurements could have been taken at any depth within each bed and assign one velocity per bed per iteration. We assume that grains could be organized anywhere between their strongest and weakest configurations. Finally, we infer changes to the sediment microstructure by comparing measured versus predicted seismic velocities (Bachrach & Avseth, 2008).

3. Results

3.1. Sediment Age and Deposition Rate

All analyzed Port Royal Beach sediments were deposited between 1692 and 2017. During this time, the shoreline prograded at an average rate of 0.3–0.48 m/year except between the years 1782–1786, 1873–1888, and 1968–1975, which experienced shoreline erosion (Figure S2). The highest and lowest progradation rates occurred between 1951 and 1968 (4.6 ± 0.24 m/year) and 1692–1782 (0.3 ± 0.06 m/year), respectively. Progradation rates during the deposition of the sediments at sites 1–4 were 1.05 ± 0.1, 4.6 ± 0.24, 2.3 ± 0.11, and 1.18 ± 0.0 m/year, respectively (Figure S2).

Analysis of the time contours created by shoreline positions and slopes reveals (Figures 1 and S1) that sites 1–4s' sediments were deposited within the last ~180 years. Site 1–4s' sediments were deposited between 1988-2016, 1956–1974, 1909–1923, and 1837–1862, respectively. During these periods, average sedimentation rates within the upper 2 m of the subsurface ranged from 5 to 25 cm/year. The average calculated sedimentation rates at sites 1–4 is 6–7, 9–11, 14–25, and 5–11 cm/year, indicating that sedimentation rates were fastest during the deposition of sites 2 and 3.

3.2. Sediment Physical Properties

The sediment type, subsurface stratigraphy, ground surface condition, and water table depth are similar between study sites. Specifically, sites 1–4 are mostly made up of olive, white, yellow, and tan colored siliciclastic sands stratified into individual beds based on grain sizes, mineralogy, porosities, and bulk densities (Figure 2). There are 9, 8, 7, and 7 individual beds at sites 1–4, respectively. Grass has grown atop sites 3–4, but its roots are not anchored more than 5 cm beneath the subsurface (Figures 1 and 2). The water table was between 1.9 and 2.2 m at all sites during trenching.

The composition (mineralogy, cement fraction, grain size, and grain shape) of the sediments at sites 1–4 are similar. The minerals are predominantly albite, quartz, and calcite; grains are rounded to well-rounded, mostly spherical, and their sizes range from coarse to very coarse sands (Figure 3). When uncertainties are considered, statistical analyses reveal that it is more probable that the average values of these physical properties are indistinguishable (within a 50-50 probability) from each other than that they change between sites. The lone exception is a 0.82 probability that site 1's bulk modulus is larger than sites 2–3s'. The higher bulk modulus at site 1 reflects a relatively larger percentage of albite at site 1, which is 77.2% compared to sites 2–4s' average albite percentages of 45.9%, 45.7%, and 63.4%, respectively (Table S1).

Average porosities and bulk densities are constant within an average ~5% uncertainty, with sites 2–4s' porosities and bulk densities being respectively within 0.01 and 0.04–0.14 g/cm^3 of site 1's. Though differences exist at the individual depth levels, statistical analyses also show no detectable increasing trends with time across all four sites either as a function of depth or as a function of the averages at each site. Instead, the analyses show

that it is more probable that these physical properties are also indistinguishable between sites as the probabilities that these physical properties increase or decrease with age are within 0.1–0.17 of 0.5 probabilities (i.e., a 50:50 chance). The pores are filled with relatively small water quantities (0–0.6% with a mean of 0.1%). The saturation percentages at sites 1-3 are statistically indistinguishable as a function of depth (Figure 3j), whereas there is a 0.35 probability that site 1–3s' water saturations are higher than site 4's (Table S1).

3.3. Sediments' Observed and Predicted Seismic Velocities

All measured seismic velocities (i.e., phase velocities of the surface waves, V_p, and V_s) increase between sites 1–2 and 3–4 (Figures 2e–2g). Seismic velocities are indistinguishable between sites 1 and 2 and between

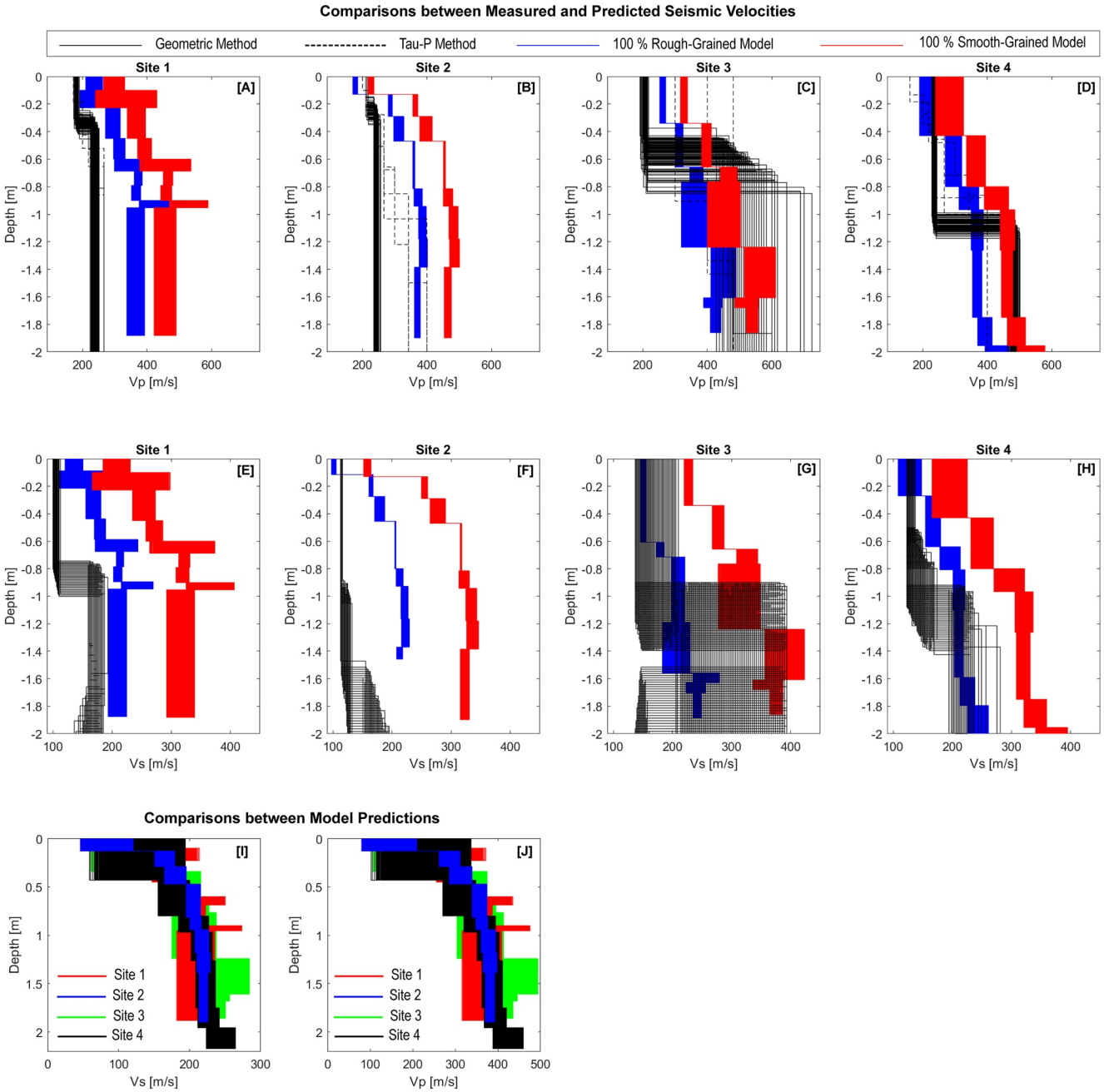

Figure 4. (a–h) Measured versus modeled velocities. (i–j) Comparisons between all modeled velocities.

sites 3 and 4. Changes to V_p show the most complexity in space and time (Figures 2f and 2g). Within the upper 1 m, turning wave velocity inversion reveals that V_p increases from sites 1 to 3 (Figure 2g). At the surface, V_p for site 4 is lower than at sites 1–3 but becomes faster than sites 1–2 with depth (starting at 1 m). Turning wave velocity results also show that V_p increases with time between 1 and 2 m. In contrast, the first-break geometric method shows that V_p in the upper 0.3 m does not increase with time (Figure 2f) and that V_p within the upper 0.3–1 m is roughly the same but increases with time between sites 1–2 and 3–4 at depths between 1 and 2 m. Overall, the V_p reveals a clear increasing V_p trend between sites 1–2 and 3–4 can only be resolved at depths of 1–2 m. V_s increases faster than V_p.

Rock physics models predict that seismic velocities are statistically indistinguishable at all sites (Figures 4i and 4j). Misfits between modeled and observed seismic velocities decrease with age, and models assuming infinite slip at all grain contacts (i.e., 100% smooth grain models) generally perform better than those assuming no slip at grain contacts (i.e., 100% rough grain models) (Figure 4). The 100% rough grain models overpredict velocities except for V_p at site 3 and below 1.2 m at site 4 (Figure 4).

4. Discussion

The relationships between measured and modeled seismic velocities at Port Royal Beach sometime conflict. Below, we demonstrate that changes to the measured physical properties do not explain the discrepancies in measured and modeled velocities. Instead, we propose that velocities increase with age due to grain reorganization, which increases the sands' elastic moduli.

Spatiotemporal increases to seismic velocities at Port Royal Beach (Figure 2) provide evidence that at least one physical property at Port Royal Beach changes with age. Variations and uncertainties in the average mineral moduli, porosity, bulk density, fluid saturation, and cement fraction alone cannot explain increases to seismic velocities as (a) there are no sustained and statistically significant changes in the site-wide averages of these properties and (b) rock physics model-predicted velocities are statistically indistinguishable when the combined effects of all variations (average or at individual depth levels) in these properties are considered (Figures 4i and 4j). We discard patchy fluid saturation because fluid saturation is too small (0%–0.6%) to induce seismic velocities changes that we observe (~100–250 m/s) (Figures 2e, 2f, 3j, and 4; Gassmann, 1951). We also discard porosity reduction and pore space cement because the rock physics models estimate that, when all else is equal, at least a 20%–30% decrease in porosity at sites 3–4 is needed to account for seismic velocity increases. It is unlikely that all cements are at grain contacts and or surround the grains because this would lead to seismic velocities that are larger (by ~500–1,000 m/s) than what we measure (Avseth et al., 2009). We are skeptical that a mixed distribution of cements (some within pore spaces and some at contacts) is responsible for increasing velocities because there are no statistically significant changes to cement percentage with time, the depositional condition at the sites has remained relatively constant with time (Goreau & Burke, 1966), and assuming that cements are within the pore spaces better predict seismic velocities at all sites.

Instead of changes to porosity and or cement fraction, an alternative hypothesis is that grain contact force distribution becomes more uniform with time and is responsible for increasing seismic velocities at Port Royal Beach. Support for this hypothesis comes from the observations that the models' misfits decrease with age, a finding which implies that the primary model assumptions (i.e., grains are identical and forces are equally distributed between grains) are more appropriate in the older sands. Observations that the 100% smooth grain models predict V_p and V_s more accurately than the rough grain models at sites 1–2 but begins to underpredict V_p beneath 1.2 m at site 4 are also instructive. These results indicate that increases in grain-contact friction are unlikely to be the primary or only cause of the observed time-dependent increases to seismic velocities at Port Royal Beach (Figures 4 and 5; Walton, 1987). Seismic velocity increases could, therefore, be caused by a combination of increases in the uniformity of distributed grain-contact forces and relatively smaller changes to friction at grain contacts (Figures 4 and 5).

Changes to grain contact forces can only occur if grains undergo microstructural re-adjustments (e.g., grain rolling, sliding, and rotating) with time. Grain re-adjustments may be induced by several processes, including but not limited to natural and anthropogenically introduced stresses such as earthquakes,

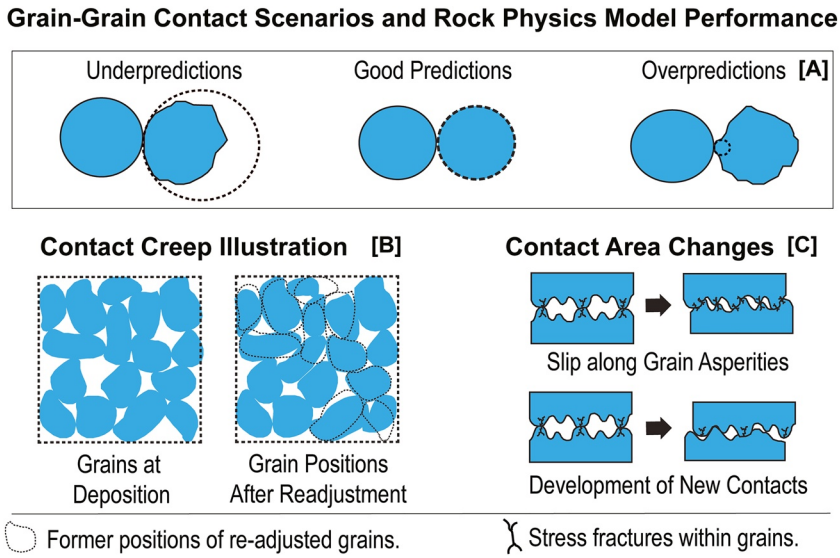

Figure 5. (a) Grain contact scenarios and their effects on model predictions (Bachrach & Avseth, 2008). Dotted lines define circles associated with the grains' radii of curvatures. (b-c) Contact creep illustrations with two possible resulting contact scenarios (Wang, 2017).

sub-surface fluid flow during intense rainfall, nearshore seawater waves, and human activities that vibrate sands. Grain re-adjustments can also occur via contact creep, which is defined as microstructural grain re-adjustments that occur (without significant external forcing) along naturally existing grain asperities or localized instabilities (Figure 5) as a mean of reducing potential energy within granular systems. The former groups of re-adjustment processes (e.g., vibration loading processes such as earthquakes or waves hitting the coasts) are often accompanied by porosity reduction, whereas contact creep increases the elastic moduli of sands without significantly (>3%) reducing their porosities (Kuhn & Mitchell, 1993; Mitchell, 2008; Wang et al., 2008).

Contact creep in clean sands are primarily influenced by viscofrictional grain contact forces, porosity, surface roughness, asperity, and contact area (Bowman & Soga, 2003; Kuhn & Mitchell, 1993; Mitchell, 2008; Wang et al., 2008). Higher grain roughness and asperity lead to smaller grain contact areas and higher viscofrictional contact forces, which promote grain micro-fracturing, grain plastic deformation, and increased mechanical instabilities at grain contacts (Kuhn & Mitchell, 1993; Wang et al., 2008). Contacting grains re-adjust (i.e., slip, slide, or rotate) when they overcome viscofrictional contact forces at energetically or mechanically unstable contacts (Kuhn & Mitchell, 1993). Grain re-adjustments during contact creep more significantly increase the homogeneity of grain contact force magnitudes and spatial distribution versus reducing porosity (Kuhn & Mitchell, 1993; Wang et al., 2008). Supporting these findings, discrete element models and lab-tests performed on sands at confining pressures of 400–500 kPa show that, in the absence of external forcing, contact creep-induced contact force homogenization alone can lead to increases in sediment elastic moduli that cannot be solely attributed to porosity reduction, which is typically less than 1.7% when modeled (Bowman & Soga, 2003; Wang et al., 2008). The exact mechanism for why contact creep preferentially leads to grain contact force homogenization is unclear (Mitchell, 2008). One hypothesis is that the relatively lower effective stresses during contact creep preclude grains from transporting the distances needed for significant porosity reduction but are sufficient for increasing grain contact forces—that is, grains can more efficiently achieve mechanical stability by increasing the forces at existing contacts and or the contact areas between the same or neighboring grains (Figure 5).

It is unclear whether the results from the above-described contact creep discrete element models and lab tests represent one-to-one relationships with the lower effective pressure (1–28 kPa) vadose zone sands at Port Royal Beach (Bowman & Soga, 2003; Wang et al., 2008). Noteworthy, however, is that the high porosities, moderate sorting, and high sphericity at Port Royal Beach would form a relatively good environment

where grains can more freely rotate, roll, and slip along naturally existing surface asperities or at nonuniform grain contacts, thus creating more stable grain contacts between the same or previously non-contacting grains (see Figure 5; Wang et al., 2014). Also noteworthy is that when sands are unloaded from 500 to 50 kPa, grain rotations continue to occur (Bowman & Soga, 2003), suggesting that grain re-adjustments occur in relatively lower effective stress environments. Our preferred interpretation is, therefore, that contact creep-induced grain reorganization is likely leading to increases to the grain contact area and homogenization of grain contact force chains, which are the primary causes for increases to seismic velocity with time without significantly reducing porosities.

The primary finding of this work (i.e., sands experience time-dependent increases to their elastic moduli that cannot be solely explained by porosity reduction) is consistent with prior studies of spatiotemporal changes to natural and artificial sands. To our knowledge, this work represents the first natural evidence suggesting that, for at least 180 years, the shear strength, elastic moduli, and microstructure of recently deposited sands may be controlled by contact creep-induced grain reorganization that does not significantly reduce porosity. These findings imply that there is likely an intermediary process between deposition and mechanical compaction at Port Royal Beach. Here, we propose that contact creep-induced grain reorganization is also a plausible explanation for why the beach, river, and dune sands examined by Atkins and McBride (1992) experience increases in their coordination numbers with depth without significant porosity reduction. As suspected by previous studies, contact creep-induced grain reorganization is also likely responsible for why artificial sands and silt-laden dams experience increases to their elastic moduli with time without significant porosity reduction (Dumas & Beaton, 1988; Mesri et al., 1990; Mitchell & Solomayor, 1984; Troncoso & Graces, 2000). Instead of solely causing increases to grain contact friction, we propose that changes to grain contact area may also increase the elastic moduli of sands. Since the microstructure of shallow sands in the upper 2–12 meters controls subsurface fluid flow, shear strength, and thus resistance to earthquake-triggered liquefaction (e.g., Martin et al., 1975), an implication of our study is that contact-creep is more dominant than porosity-reducing mechanical compaction at controlling liquefaction. Lastly, we predict that our main findings are likely replicable at other Holocene beaches because Port Royal Beach's porosities, bulk densities, grain sizes, and coastline progradation rates (Figure S1) are similar to other Holocene beaches across the world (Atkins & McBride, 1992; Gunn et al., 2006; McDonald, 2013; McLean & Kirk, 1969; Prodger et al., 2016; Pryor, 1973).

5. Conclusions

Port Royal Beach, Jamaica, is composed of highly porous albite and quartz-rich sands with less than 3% carbonate cementation. The sands were deposited between 1692 and the present. The compressional and shear wave velocities at the beach increase with sediment age and are unaccompanied by any sustained and statistically significant or detectable increases or decreases to porosity, bulk density, grain size, sorting, and cement fraction with time. Rock physics models more accurately predict seismic velocities for older and deeper buried sands, a discrepancy that cannot be explained when the most liberal uncertainties are employed at each study site. Together with the sediment property and seismic velocity analyses, the rock physics model results imply that increasing velocities are better explained by grain reorganization (e.g., rotation and slippage), leading to an increase in the elastic moduli of the sediment matrix with time since deposition.

Our observations are consistent with recent (within the last 40 years) findings by geotechnical engineers, who recognized that artificial sands experience a temporal (within minutes and last for decades) increase in their shear moduli that is accompanied by a relatively small (<3%) decrease in porosity. Here, we provide evidence that this process may also include changes to bulk moduli, occurs within naturally occurring siliciclastic sands, and occurs on not just decadal but on centennial time scales as well. We propose that this process occurs via contact creep primarily, leads to an increase in the magnitude and uniformity of distributed grain contact forces, and represents an intermediary process between sediment deposition and mechanical compaction.

Data Availability Statement

The seismic refraction profiles used in this study are publicly available at https://doi.org/10.5281/zenodo.4564867.

Acknowledgments
The authors thank L. Brown, J. Burton, S. Cuff, W. Harding, S. Hoppins, D. Kennedy, R. Mitchell, P. Parchment, and D. Phillpotts for helping during field surveys. The authors collected seismic refraction data using Passcal Instrument Center's equipment. The Society of Exploration Geophysicists Geoscientists without Borders Grant and the Institute for Earth, Science, and Man at Southern Methodist University partially supported this work.

References

Athy, L. F. (1930). Density, porosity, and compaction of sedimentary rocks. *AAPG Bulletin*, *14*(1), 1–24.
Atkins, J. E., & McBride, E. F. (1992). Porosity and Packing of Holocene River, Dune, and beach sands (1). *AAPG Bulletin*, *76*. https://doi.org/10.1306/bdff87f4-1718-11d7-8645000102c1865d
Avseth, P., Jørstad, A., van Wijngaarden, A.-J., & Mavko, G. (2009). Rock physics estimation of cement volume, sorting, and net-to-gross in North Sea sandstones. *The Leading Edge*, *28*, 98–108. https://doi.org/10.1190/1.3064154
Bachrach, R., & Avseth, P. (2008). Rock physics modeling of unconsolidated sands: Accounting for nonuniform contacts and heterogeneous stress fields in the effective media approximation with applications to hydrocarbon exploration. *Geophysics*, *73*, E197–E209. https://doi.org/10.1190/1.2985821
Batemann, H. (1910). Die Lösung der Integralgleichung, welche die Fortpflanzungsgeschwindigkeit einer Erdbebenwelle im Inneren der Erde mit den Zeiten verbindet, die die Störung braucht, um zu verschiedenen Stationen auf der Erdoberfläche zu gelangen. *Physikalische Zeitschrift*, *11*, 96–99.
Biot, M. A. (1956). Theory of propagation of elastic waves in a fluid-saturated porous solid. II. Higher frequency range. *The Journal of the Acoustical Society of America*, *28*, 179–191. https://doi.org/10.1121/1.1908241
Bowman, E., & Soga, K. (2003). Creep, ageing and microstructural change in dense granular materials. *Soils and Foundations*, *43*, 107–117. https://doi.org/10.3208/sandf.43.4_107
Cox, B. R., & Teague, D. P. (2017). Erratum: Layering ratios: A systematic approach to the inversion of surface wave data in the absence of a-priori information. *Geophysical Journal International*, *211*, 378. https://doi.org/10.1093/gji/ggx319
Crowe, A., & Milne, J. (2013). Relationship between dry and wet beach ecosystems and E. coli levels in groundwater below beaches of the Great Lakes, Canada. *IAH—Selected Papers on Hydrogeology Groundwater and Ecosystems*, *18*, 237–251. https://doi.org/10.1201/b15003-20
Digerfeldt, G., & Hendry, M. D. (1987). An 8000 year Holocene sea-level record from Jamaica: Implications for interpretation of Caribbean reef and coastal history. *Coral Reefs*, *5*(4), 165–169. https://doi.org/10.1007/bf00300959
Dugan, B., & Flemings, P. B. (2002). Fluid flow and stability of the US continental slope offshore New Jersey from the Pleistocene to the present. *Geofluids*, *2*, 137–146. https://doi.org/10.1046/j.1468-8123.2002.00032.x
Dumas, J. C., & Beaton, N. F. (1988). Discussion of "Practical problems from surprising soil behavior" by James K. Mitchell (March, 1986, Vol. 112, No. 3). *Journal of Geotechnical Engineering*, *114*, 367–368. https://doi.org/10.1061/(asce)0733-941010.1061/(asce)0733-9410(1988)114:3(367)
Dutta, T., Mavko, G., Mukerji, T., & Lane, T. (2009). Compaction trends for shale and clean sandstone in shallow sediments, Gulf of Mexico. *The Leading Edge*, *28*, 590–596. https://doi.org/10.1190/1.3124935
Folk, R. L., & Ward, W. C. (1957). Brazos river bar [Texas]; a study in the significance of grain size parameters. *Journal of Sedimentary Research*, *27*, 3–26. https://doi.org/10.1306/74d70646-2b21-11d7-8648000102c1865d
Fuller, M. L. (1907). Notes on the Jamaica earthquake. *The Journal of Geology*, *15*, 696–721. https://doi.org/10.1086/621461
Gassmann, F. (1951). *Uber di elastizitat poroser median: Vier* (Vol. 96, pp. 1–23). der Natur Gesellschaft in Zurich.
Goreau, T., & Burke, K. (1966). Pleistocene and Holocene geology of the island shelf near Kingston, Jamaica. *Marine Geology*, *4*, 207–224. https://doi.org/10.1016/0025-3227(66)90021-1
Gunn, D. A., Pearson, S. G., Chambers, J. E., Nelder, L. M., Lee, J. R., Beamish, D., et al. (2006). An evaluation of combined geophysical and geotechnical methods to characterize beach thickness. *The Quarterly Journal of Engineering Geology and Hydrogeology*, *39*, 339–355. https://doi.org/10.1144/1470-9236/05-038
Haskell, N. A. (1951). The dispersion of surface waves on multilayered media. *Bulletin of the Seismological Society of America*, *43*(1), 1–18.
Herglotz, G. (1907). Über das Benndorf'sche Problem der Fortpflanzungsgeschwindigkeit der Erdbebenstrahlen. *Physikalische Zeitschrift*, *8*, 145–147.
Hill, R. (1952). The elastic behaviour of a crystalline aggregate. *Proceedings of the Physical Society*, *65*, 349–354. https://doi.org/10.1088/0370-1298/65/5/307
Hillier, S. (2000). Accurate quantitative analysis of clay and other minerals in sandstones by XRD: Comparison of a rietveld and a reference intensity ratio (RIR) method and the importance of sample preparation. *Clay minerals*, *35*(1), 291–302.
Katahara, K. W. (1996). Clay mineral elastic properties. In *SEG Technical Program Expanded Abstracts 1996*. Society of Exploration Geophysicists. https://doi.org/10.1190/1.1826454
Kuhn, M. R., & Mitchell, J. K. (1993). New perspectives on soil creep. *Journal of Geotechnical Engineering*, *119*(3), 507–524. https://doi.org/10.1061/(asce)0733-9410(1993)119:3(507)
Lundegard, P. D. (1992). Sandstone porosity loss; a "big picture" view of the importance of compaction. *Journal of Sedimentary Research*, *62*, 250–260. https://doi.org/10.1306/D42678D4-2B26-11D7-8648000102C1865D
Makse, H. A., Gland, N., Johnson, D. L., & Schwartz, L. (2004). Granular packings: Nonlinear elasticity, sound propagation, and collective relaxation dynamics. *Physical Review E—Statistical Physics, Plasmas, Fluids, and Related Interdisciplinary Topics*, *70*. https://doi.org/10.1103/physreve.70.061302
Makse, H. A., Gland, N., Johnson, D. L., & Schwartz, L. M. (1999). Why effective medium theory fails in granular materials. *Physical Review Letters*, *83*, 5070–5073. https://doi.org/10.1103/physrevlett.83.5070
Martin, G. R., Seed, H. B., & Finn, W. D. L. (1975). Fundamentals of liquefaction under cyclic loading. *Journal of the Geotechnical Engineering Division*, *101*(5), 423–438. https://doi.org/10.1061/AJGEB6.0000164
McDonald, R., Wright, V., Hornbach, M. J., Carris, G., Flynn, C., Frone, Z., et al. (2013). New insights into geohazard risks in Jamaica, Haiti, and the Dominican Republic: A compendium of recent Geoscientists without Borders results. Paper presented at the *SEG Technical Program Expanded Abstracts 2013*. Houston, TX. Society of Exploration Geophysicists. https://doi.org/10.1190/segam2013-1293.1
Mclean, R. F., & Kirk, R. M. (1969). Relationships between grain size, size-sorting, and foreshore slope on mixed sand - Shingle beaches. *New Zealand Journal of Geology and Geophysics*, *12*, 138–155. https://doi.org/10.1080/00288306.1969.10420231

Mesri, G., Feng, T. W., & Benak, J. M. (1990). Postdensification penetration resistance of clean sands. *Journal of Geotechnical Engineering*, *116*, 1095–1115. https://doi.org/10.1061/(asce)0733-9410(1990)116:7(1095)

Mindlin, R. D. (1949). Compliance of elastic bodies in contact. *Journal of Applied Mechanics*, *16*, 259–268. https://doi.org/10.1007/978-1-4613-8865-4_2410.1115/1.4009973

Mitchell, J. K. (2008). Aging of sand–a continuing enigma? Paper presented at the *6th International Conference on Case Histories in Geotechnical Engineering*, Arlington, VA. https://doi.org/10.1061/40962(325)15

Mitchell, J. K., & Solymar, Z. V. (1984). Time-dependent strength gain in freshly deposited or densified sand. *Journal of Geotechnical Engineering*, *110*, 1559–1576. https://doi.org/10.1061/(ASCE)0733-9410(1984)110:11(1559)

Morelock, J. (1969). Shear strength and stability of continental slope deposits, western Gulf of Mexico. *Journal of Geophysical Research*, *74*, 465–482. https://doi.org/10.1029/jb074i002p00465

Murphy, W. F. (1982). *Effects of microstructure and pore fluids on the acoustic properties of granular sedimentary materials*. (Doctoral dissertation). Stanford, CA: Stanford University.

Park, C. B., Miller, R. D., & Xia, J. (1999). Multichannel analysis of surface waves. *Geophysics*, *64*, 800–808. https://doi.org/10.1190/1.1444590

Prasad, M., Kopycinska, M., Rabe, U., & Arnold, W. (2002). Measurement of Youngs modulus of clay minerals using atomic force acoustic microscopy. *Geophysical Research Letters*, *29*. https://doi.org/10.1029/2001gl014054

Prodger, S., Russell, P., Davidson, M., Miles, J., & Scott, T. (2016). Understanding and predicting the temporal variability of sediment grain size characteristics on high-energy beaches. *Marine Geology*, *376*, 109–117. https://doi.org/10.1016/j.margeo.2016.04.003

Pryor, W. A. (1973). Permeability-porosity patterns and variations in some holocene sand bodies. *AAPG Bulletin*, *57*. https://doi.org/10.1306/819a4252-16c5-11d7-8645000102c1865d

Revil, A., Grauls, D., & Brévart, O. (2002). Mechanical compaction of sand/clay mixtures. *Journal of Geophysical Research*, *107*, 11–1. https://doi.org/10.1029/2001jb000318

Richart, F. E., Hall, J. R., & Woods, R. D. (1970). Vibrations of soils and foundations. In F. E. Richart, R. D. Woods, J. R. Hall (Eds.). *Prentice-Hall International Series in Theoretical and Applied Mechanics*: Englewood Cliffs, NJ. Prentice-Hall.

Thomson, W. T. (1950). Transmission of elastic waves through a stratified solid medium. *Journal of Applied Physics*, *21*(2), 89–93. https://doi.org/10.1063/1.1699629

Troncoso, J. H., & Garcés, E. (2000). Ageing effects in the shear modulus of soils. *Soil Dynamics and Earthquake Engineering*, *19*, 595–601. https://doi.org/10.1016/s0267-7261(00)00066-x

Vousdoukas, M. I., Velegrakis, A. F., & Plomaritis, T. A. (2007). Beachrock occurrence, characteristics, formation mechanisms and impacts. *Earth-Science Reviews*, *85*, 23–46. https://doi.org/10.1016/j.earscirev.2007.07.002

Walton, K. (1987). The effective elastic moduli of a random packing of spheres. *Journal of the Mechanics and Physics of Solids*, *35*, 213–226. https://doi.org/10.1016/0022-5096(87)90036-6

Wang, Y.-H., Lau, Y. M., & Gao, Y. (2014). Examining the mechanisms of sand creep using DEM simulations. *Granular Matter*, *16*, 733–750. https://doi.org/10.1007/s10035-014-0514-4

Wang, Y.-H., Xu, D., & Tsui, K. Y. (2008). Discrete element modeling of contact creep and aging in sand. *Journal of Geotechnical and Geoenvironmental Engineering*, *134*, 1407–1411. https://doi.org/10.1061/(asce)1090-0241(2008)134:9(1407)

Wang, Z. (2017). *Contact maturing and aging of silica sand, (Doctoral dissertation)*. Ann Arbor, MI: University of Michigan. Retrieved from http://hdl.handle.net/2027.42/136992

Wang, Z. Z., Wang, H., & Cates, M. E. (1998). Elastic properties of solid clays. Paper presented at *SEG Technical Program Expanded Abstracts 1998*. Society of Exploration Geophysicists. https://doi.org/10.1190/1.1820064

Wathelet, M., Jongmans, D., & Ohrnberger, M. (2004). Surface-wave inversion using a direct search algorithm and its application to ambient vibration measurements. *Near Surface Geophysics*, *2*, 211–221. https://doi.org/10.3997/1873-0604.2004018

Wiechert, E. (1910). Bestimmung des Weges von Erdbebenwellen. I. Theoretisches. *Physikalische Zeitschrift*, *11*, 294.

Wiechert, E. & Geiger, L. (1901). Bestimmung des Weges von Erdbebenwellen im Erdinneren. *Physikalische Zeitschrift*, *11*, 394–411.

Wright, V., Hornbach, M., Brown, L., McHugh, C., & Mitchell, S. (2019). Neotectonics of southeast Jamaica derived from marine seismic surveys and gravity cores. *Tectonics*, *38*, 4010–4026. https://doi.org/10.1029/2019tc005806

Zheng, J., & Hryciw, R. D. (2015). Traditional soil particle sphericity, roundness and surface roughness by computational geometry. *Géotechnique*, *65*(6), 494–506.